

Hemodynamic impairments within individual watershed areas in asymptomatic carotid artery stenosis by multimodal MRI

Journal of Cerebral Blood Flow & Metabolism

0(0) 1–17

© The Author(s) 2020



Article reuse guidelines:

sagepub.com/journals-permissions

DOI: 10.1177/0271678X20912364

journals.sagepub.com/home/jcbfm

Stephan Kaczmarz^{1,2,3} , Jens Göttler^{1,2,3,4} , Jan Petr⁵ ,
Mikkel Bo Hansen⁶ , Kim Mouridsen⁶, Claus Zimmer¹,
Fahmeed Hyder³ and Christine Preibisch^{1,2,7}

Abstract

Improved understanding of complex hemodynamic impairments in asymptomatic internal carotid artery stenosis (ICAS) is crucial to better assess stroke risks. Multimodal MRI is ideal for measuring brain hemodynamics and has the potential to improve diagnostics and treatment selections. We applied MRI-based perfusion and oxygenation-sensitive imaging in ICAS with the hypothesis that the sensitivity to hemodynamic impairments will improve within individual watershed areas (iWSA). We studied cerebral blood flow (CBF), cerebrovascular reactivity (CVR), relative cerebral blood volume (rCBV), relative oxygen extraction fraction (rOEF), oxygen extraction capacity (OEC) and capillary transit-time heterogeneity (CTH) in 29 patients with asymptomatic, unilateral ICAS (age 70.3 ± 7.0 y) and 30 age-matched healthy controls. In ICAS, we found significant impairments of CBF, CVR, rCBV, OEC, and CTH (strongest lateralization $\Delta\text{CVR} = -24\%$), but not of rOEF. Although the spatial overlap of compromised hemodynamic parameters within each patient varied in a complex manner, most pronounced changes of CBF, CVR and rCBV were detected within iWSAs (strongest effect $\Delta\text{CVR} = +117\%$). At the same time, CTH impairments were iWSA independent, indicating widespread dysfunction of capillary-level oxygen diffusivity. In summary, complementary MRI-based perfusion and oxygenation parameters offer deeper perspectives on complex microvascular impairments in individual patients. Furthermore, knowledge about iWSAs improves the sensitivity to hemodynamic impairments.

Keywords

Asymptomatic internal carotid artery stenosis, cerebrovascular disease, hemodynamics, individual watershed areas, magnetic resonance imaging

Received 6 September 2019; Revised 23 December 2019; Accepted 7 February 2020

Introduction

Asymptomatic internal carotid artery stenosis (ICAS) is a major public health issue. It causes approximately 10% of all strokes¹ and is also associated with cognitive decline.^{2,3} While effective interventions are available, they come with substantial risks.⁴ In this regard, identification of individual patients with high stroke risk who could benefit from a more invasive treatment is crucial. Multimodal magnetic resonance imaging (MRI) of perfusion and oxygenation is highly promising to understand hemodynamic dysfunctions of ICAS patients and to gain deeper insights into the pathology.

¹Department of Neuroradiology, School of Medicine, Technical University of Munich (TUM), Munich, Germany

²TUM Neuroimaging Center (TUM-NIC), Technical University of Munich (TUM), Munich, Germany

³MRRC, Yale University, New Haven, CT, USA

⁴Department of Radiology, School of Medicine, Technical University of Munich (TUM), Munich, Germany

⁵PET Center, Institute of Radiopharmaceutical Cancer Research, Helmholtz-Zentrum Dresden-Rossendorf, Dresden, Germany

⁶Center of Functionally Integrative Neuroscience, Aarhus University, Aarhus, Denmark

⁷Clinic for Neurology, School of Medicine, Technical University of Munich (TUM), Munich, Germany

Corresponding author:

Stephan Kaczmarz, Department of Neuroradiology, School of Medicine, Technical University of Munich, Ismaninger Str. 22, 81675 München, Germany.

Email: stephan.kaczmarz@tum.de

This could be used for personalized stroke risk assessment⁵ and improved treatment guidelines⁶ to reduce overall risk of ischemia. While perfusion deficits in ICAS have been investigated intensively,^{7–11} the relationships among different types of hemodynamic impairments in individual patients remain unclear and need further characterization.⁵ Furthermore, improved sensitivity to even subtle hemodynamic changes is necessary. It is already known that border zones between perfusion territories are most vulnerable to hemodynamic impairment.^{12,13} ICAS significantly increases the spatial variability of these watershed areas,¹⁴ e.g. by collateral flow.¹⁵ Therefore, hemodynamic parameter evaluation within individually defined watershed areas (iWSA)¹⁴ appears especially promising in ICAS to increase the sensitivity.

Atherosclerotic plaque in ICAS causes decreased cerebral perfusion pressure (CPP).¹⁶ Its impact on hemodynamics has been studied extensively.^{5,10,17} In 1987, Powers et al. characterized hemodynamic changes caused by reduced CPP in two sequential stages.¹⁸ First, autoregulatory vasodilation causes increased cerebral blood volume (CBV) and concomitantly reduced cerebrovascular reactivity (CVR). Second, when autoregulation can no longer compensate for further decreases in CPP, the cerebral blood flow (CBF) decreases. Consequently, an increase in the oxygen extraction fraction (OEF) helps with sustaining the oxidative metabolism, thereby preventing strokes. However, experimental evidence has partially contradicted this simple picture. A positron emission tomography (PET) study in patients with carotid occlusions demonstrated increased OEF already at supposedly normal CBV.¹⁰ A study in an animal ischemia model suggested reduced CBF already within the autoregulatory range.¹⁹ Recent MRI studies have also reported unchanged OEF with a decreased CBF.^{7,11} This mismatch between the OEF and CBF changes might indicate microscopic variations of oxygen diffusivity from the capillary bed to brain tissue, as proposed by Hyder et al.^{20–22}

While earlier PET studies revealed important information on ICAS-related hemodynamic impairments, the clinical applicability is restricted by limited availability, methodological complexity, radioactive tracer application and high costs of ¹⁵O PET. Emerging MRI methods now allow a comprehensive evaluation of tissue perfusion and oxygenation, and a non-invasive measurement of up to six hemodynamic parameters within a single session. This provides new possibilities to derive comprehensive information about the localization and extent of hemodynamic impairments. CBF and CVR can be measured non-invasively by pseudo-continuous arterial spin labeling (pCASL)²³ and breath-hold functional MRI

(BH-fMRI),²⁴ respectively. Previous studies have already demonstrated that CVR can help to predict the stroke risk.^{25,26} Using multi-parametric quantitative BOLD (mq-BOLD) imaging, the relative oxygen extraction fraction (rOEF) can be modeled based on separate mapping of quantitative T₂ and T₂^{*}, together with relative CBV (rCBV) using dynamic susceptibility contrast (DSC) imaging.²⁷ In addition to perfusion and mq-BOLD-based oxygenation imaging, a parametric modeling approach for DSC data, introduced by Jespersen and Østergaard, offers the possibility of exploring capillary dysfunction in ICAS.^{28–30} Here, capillary transit-time heterogeneity (CTH) and oxygen extraction capacity (OEC), which describes the maximum possible OEF, are modeled additionally from DSC data. In combination, these six parameters are highly promising to evaluate these novel quantitative physiological MRI techniques towards personalized stroke risk assessment.⁵

The aim of this study was therefore to gain deeper insights into the complex interplay of hemodynamic impairments in ICAS by measuring six microvascular MRI biomarkers (CBF, CVR, rCBV, rOEF, OEC and CTH) in patients with asymptomatic ICAS and age-matched healthy controls (HC). Moreover, we aimed to study the perfusion and oxygenation sensitive parameters inside and outside the iWSAs. We hypothesized that combinations of these perfusion and oxygenation parameters and evaluation within subject-specific iWSAs¹⁴ will improve the sensitivity to hemodynamic impairments in ICAS.

Methods

Participants

Fifty-nine subjects participated in this prospective study. We scanned 29 patients with asymptomatic, unilateral, high-grade, extracranial ICAS (>70% according to NASCET³¹ confirmed by duplex ultrasonography; 10 females; mean age 70.3 ± 7.0 years; without TIA/stroke-like symptoms; see Table 1) and 30 age-matched HCs (17 females; mean age 70.2 ± 4.8 years). Asymptomatic ICAS patients were identified by incidental findings. Healthy controls were enrolled by word-of-mouth advertisement from May 2015 until May 2017. The examination included medical history, basic neurological examination and MRI. Exclusion criteria were any neurological, psychiatric or systemic diseases, clinically remarkable structural MRI findings (e.g. territorial stroke lesions, bleedings, or a history of brain surgery), severe chronic kidney disease or MR contraindications. The study was approved by the medical ethical board of the Klinikum rechts der Isar, in line with Human Research

Table 1. Clinical characteristics for ICAS patients and healthy controls.

	Patients (n = 29)	Healthy Controls (n = 30)	p
Age (years)	70.3 ± 7.0 y	70.2 ± 4.8 y	0.94
Female sex (No. (%))	10 (34%)	17 (57%)	0.09
Stenotic degree (NASCET)	81.2 ± 10.1 %	–	
Stenosis left-/right-sided (No.)	10/19	–	
Good collateralization	17 (59%)	20 (67%)	0.34
Smoking (No. (%))	15 (52%)	11 (37%)	0.25
Mean pack-years in smokers	34.9 ± 21.9	21.5 ± 15.3	
Hypertension (No. (%))	23 (79%)	16 (53%)	0.04*
Mean BP (mmHg, sys./dias.)	154 ± 23/86 ± 10	140 ± 20/84 ± 7	0.01*/0.42
Body mass index	26.3 ± 4.7	26.6 ± 4.2	0.76
Diabetes (No. (%))	8 (28%)	2 (7%)	0.03*
Medication (No. (%))			
Antiplatelets	26 (90%)	6 (20%)	<0.01*
Statins	19 (66%)	7 (23%)	0.10
Antihypertensives	20 (69%)	12 (40%)	0.19
CHD/PAOD (No. (%))	16 (55%)	6 (20%)	<0.01*
MMSE	27.9 ± 2.6	28.6 ± 1.4	0.19
TMT-A (s)	49.3 ± 23.1	46.7 ± 29.7	0.72
TMT-B (s)	134.1 ± 65.5	116.9 ± 63.1	0.18
BDI	9.2 ± 9.9	8.4 ± 5.1	0.66
STAI	38.3 ± 14.8	24.5 ± 11.5	0.23

Note: Variables are represented by the mean values and standard deviations. Two-sample t-tests were used for age, BP, and body mass index. Chi-squared test for remaining group comparisons. Asterisks indicate significant group differences ($p < 0.05$). Collateralization status of the circle of Willis was assessed by the presence of ACOM and PCOMs, based on contrast agent-based angiography scans.

BDI: Beck's depression inventory; BP: blood pressure; CHD: coronary heart disease; LBT: line bisection test; MMSE: mini-mental state examination; PAOD: peripheral artery occlusive disease; STAI: state trait anxiety inventory; TMT-A/B: trail making test–A/B.

Committee guidelines of the Technical University of Munich (TUM). All participants provided informed written consent in accordance with the standard protocol approvals.

Image acquisition

The multimodal MRI protocol was performed using a clinical 3T Philips Ingenia MR-Scanner (Philips Healthcare, Best, The Netherlands) using a 16-channel head/neck and 32-channel head receive-coil. Custom patches were applied on software release R5.1.8 to optimize T_2^* imaging by macroscopic background gradient correction,^{32,33} to apply multiband imaging (MB)³⁴ and to improve pCASL by 3D GraSE readout, prolonged labeling and improved background suppression (BGS).³⁵ Details of the imaging protocol were as follows (Figure 1):

- *Structural imaging* involved T_2 -weighted FLAIR (TE = 289 ms, TR = 4800 ms, inversion delay 1650 ms, TSE factor 167, 163 slices, matrix size 224 × 224, voxel size 1.12 × 1.12 × 1.12 mm³, acquisition time 4:34 min) and T_1 -weighted MPRAGE (TE = 4 ms, TR = 9 ms, $\alpha = 8^\circ$, TI = 1000 ms, shot interval 2300 ms, SENSE AP/RL 1.5/2.0, 170 slices, matrix size 240 × 238, voxel size 1 × 1 × 1 mm³, acquisition time

5:59 min) to facilitate brain screening for lesions, their rating according to the Fazekas-score³⁶ (Rater: JG) and tissue segmentation, respectively.

- *pCASL* was performed according to the ISMRM perfusion study group consensus paper²³ and as described previously.¹¹ Since we applied single post label delay (PLD), a prolonged PLD of 2000 ms was used, which followed the consensus recommendations.²³ The other imaging parameters were: Label duration 1800 ms, 4 BGS pulses, segmented 3D GraSE readout (TE = 7.4 ms, TR = 4377 ms, $\alpha = 90^\circ$, 16 slices, TSE factor 19, echo planar imaging (EPI) factor 7, acquisition voxel size 2.75 × 2.75 × 6.0 mm³), three dynamics including a proton density weighted (PD-weighted) M_0 scan, and an acquisition time of 5:41 min.
- *BH-fMRI* was performed according to Pillai et al.²⁴ with five end-expiratory breath-holds of 15 s that were altered with 45 s of normal breathing. Imaging was performed by single-shot EPI with TE = 30 ms, TR = 1200 ms, $\alpha = 70^\circ$, MB 2, SENSE 2, 38 slices, matrix size 64 × 62, voxel size 3 × 3 × 3 mm³, acquisition time 5:48 min.
- *T_2 -mapping* was based on an eight echo gradient-spin-echo (GraSE) sequence as described previously²⁷: TE₁ = Δ TE = 16 ms, TR = 8596 ms, EPI factor

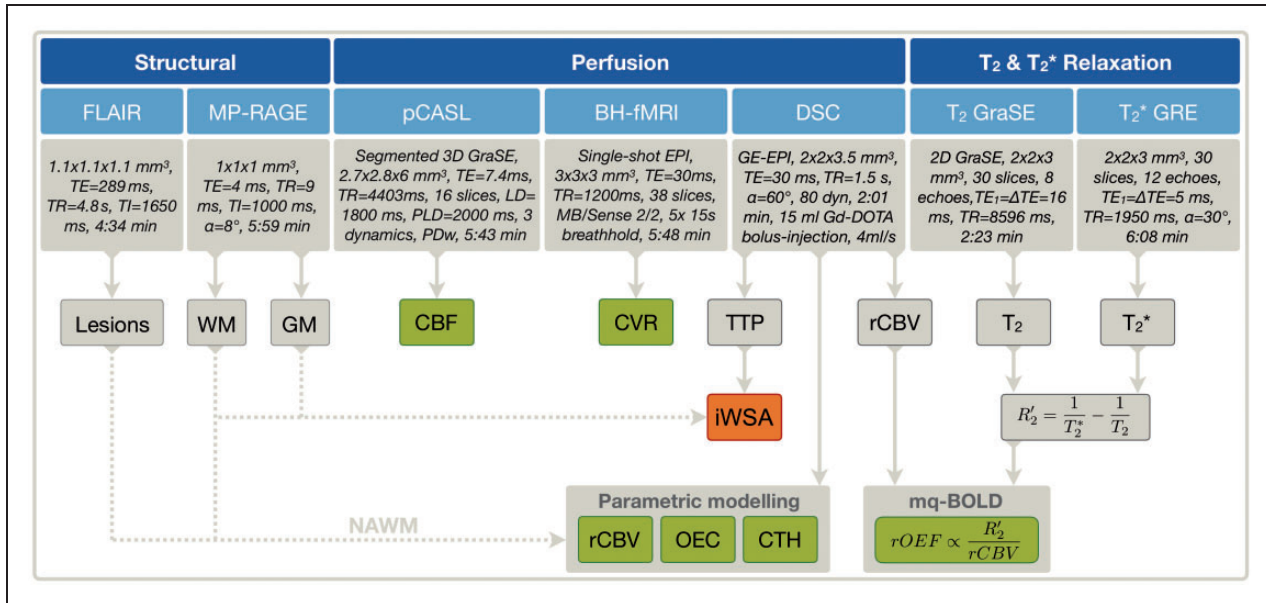


Figure 1. Overview of MRI protocol and derived parameters. Structural imaging comprised FLAIR and MP-RAGE for lesion detection and the generation of white matter (WM) and gray matter (GM) masks. Pseudo-continuous arterial spin labeling (pCASL) was applied to measure cerebral blood flow (CBF) and breath-hold fMRI (BH-fMRI) for cerebral vascular reactivity (CVR). By DSC-MRI, time to peak (TTP) maps were derived and used to generate individual watershed areas (iWSA) for each participant, which were additionally GM/WM masked. By parametric modeling, relative cerebral blood volume (rCBV), oxygen extraction capacity (OEC), and capillary transit-time heterogeneity (CTH) maps were calculated. By mq-BOLD, rOEF was modeled based on rCBV (normalized to CBV = 2.5% in NAWM), T₂ and T₂*. The iWSA-mask (orange box) was applied to each of the six hemodynamic biomarkers (green boxes) for all participants. For group level analyses, average parameter values were calculated for both hemispheres inside and outside of iWSAs in GM and WM.

47, 30 slices, gap 0.3 mm, matrix 112 × 91, voxel size 2 × 2 × 3 mm³, acquisition time 2:23 min.

- T₂*-mapping used a 12-echo gradient echo (GRE) sequence featuring exponential excitation pulses to facilitate correction of magnetic background gradients³³ and duplicate acquisition of the k-space center for motion correction,³⁷ as described previously²⁷: TE₁ = ΔTE = 5 ms, TR = 1950 ms, α = 30°, mono-polar readout, 30 slices, matrix size 112 × 92, voxel size 2 × 2 × 3 mm³, total acquisition time 6:08 min.
- DSC-MRI used dynamic acquisition of 80 single-shot gradient-echo EPI volumes (TE = 30 ms, TR = 1513 ms, α = 60°, 26 slices, voxel size 2.0 × 2.0 × 3.5 mm³, acquisition time 2:01 min) during injection of a weight-adjusted Gd-DOTA bolus (concentration 0.5 mmol/ml, dose 0.1 mmol/kg, at least 7.5 mmol per subject, flow rate 4 ml/s, injection 7.5 s after DSC imaging onset, with a 40 ml saline flush), which followed the ASFN recommendations³⁸ and as described previously.³⁹ Contrast-enhanced angiography of the arteries of the neck and the aortic arch was also performed to exclude other relevant stenoses arteries that supply

the brain. The angiography was performed before the DSC and also served as a prebolus.

Image analysis

All processing procedures used custom MATLAB programs (MATLAB R2016b, MathWorks, Natick, MA, USA) and SPM12 (Wellcome Trust Centre for Neuroimaging, UCL, London, UK). All parameter maps were screened, especially for motion artefacts (raters CP, SK), to exclude scans with low data quality from the final evaluation. The following parameter maps were calculated:

- GM and WM tissue masks were created by segmentation of MPRAGE images and thresholding of those maps with p > 0.70.
- Quantitative CBF was derived from pCASL, where label and control images were motion corrected, averaged, subtracted, and the M₀ image was included in the calculations according to Alsop et al.²³ An additional signal reduction of 25% was assumed due to the application of BGS.^{40,41} The resulting CBF maps were smoothed by a 3D Gaussian kernel with FWHM of 5 mm. CBF maps did not show

evidence of arterial transit time (ATT) artefacts¹¹ on careful visual inspection of unsmoothed CBF maps (JG, CP, SK) and as implied by a spatial coefficient of variation <0.45 according to Mutsaerts et al.⁴²

- Relative CVR maps were obtained from BH-fMRI data.²⁴ Time series data were motion corrected and CVR was measured using beta-values that were calculated by regression of a respiratory response function after correcting for a global time delay in a model-driven approach according to Vondráčková et al.⁴³
- iWSAs were defined based on temporal delays in perfusion, because of their peripheral location at the edge of vascular territories, as previously presented.¹⁴ Temporal information was obtained from DSC-based time-to-peak (TTP) maps. To this end, smoothed TTP-maps were segmented semi-automatically. Their location was confirmed by comparison with an arterial transit time atlas and assessment of perfusion territories by vessel selective ASL for a subgroup of patients as previously presented.¹⁴
- Parametric modeling of DSC-data followed the approach of Jespersen and Østergaard²⁸ with semi-automated AIF definition and yielded maps of rCBV, OEC and CTH.^{44,45} The approach is based on a single capillary model (see Figure 1 in Jespersen and Østergaard²⁸). It assumes that oxygen extraction in a single capillary depends on the transit time of blood. Thus, oxygen extraction depends on flow and the difference in plasma and tissue oxygen concentration.^{46,47} OEC is obtained by integrating single capillary contributions that are weighted by the transit time distribution of the capillaries within the capillary bed (see Eq. 1 in Jespersen and Østergaard²⁸). To this end, the probability density function of capillary transit times is parametrized as a gamma variate function (see Eq.2 in Jespersen and Østergaard²⁸), which allows estimation of CTH.^{44,45} The CBV maps were normalized to normal appearing white matter (NAWM) as previously reported,^{27,39} which yielded rCBV maps (Figure 1).
- rOEF was derived by a multi-parametric implementation for the quantification of the blood oxygenation level-dependent (BOLD) effect.²⁷ The method is based on an analytical relationship between R_2' , venous CBV and venous oxygenation that was originally derived by Yablonskiy and Haacke for randomly oriented magnetized cylinders assuming static dephasing conditions.⁴⁸ Quantitative T_2^* and T_2 parameter maps were calculated by mono-exponential fitting of the multi-echo GRE and even-echoes GraSE data, correcting influences of magnetic background gradients, motion and stimulated echoes as described previously.^{27,49} Based on

these parameter maps, $R_2' = \frac{1}{T_2^*} - \frac{1}{T_2}$ was calculated. DSC data were processed employing leakage correction^{39,50} to calculate CBV maps, which were normalized to $CBV=2.5\%$ in normal appearing WM (NAWM)⁵¹ yielding rCBV. Using the mq-BOLD approach,²⁷ rOEF was calculated as $rOEF = \frac{R_2'}{c \cdot rCBV}$ with $c = \gamma \cdot \frac{4}{3} \cdot \pi \cdot \Delta\chi \cdot B_0$ and $B_0 = 3 \text{ T}$ with $\Delta\chi = \Delta\chi_0 \cdot Hct = 0.924 \cdot 10^{-7}$, $\Delta\chi_0 = 0.264 \cdot 10^{-6}$ and the small-vessel hematocrit $Hct = 0.35$ and $\gamma = 2.675 \cdot 10^8 \text{ s}^{-1} \text{ T}^{-1}$.

While estimation of OEC from DSC-MRI relies on a vascular model,^{44,45} estimation of rOEF by mq-BOLD is based on an implementation²⁷ of an analytical model⁴⁸ describing spin dephasing, i.e. susceptibility related transverse relaxation, in the presence of randomly oriented magnetized cylinders, i.e. blood vessels containing deoxygenated blood.

Individual parameter maps were calculated in each subject's native space, as described above. Subsequently, all data (CBF, CVR, rOEF, MPRAGE, GM and WM masks) were spatially coregistered to the individual participant's DSC-data (rCBV, OEC, CTH, and iWSA) using SPM12 to maintain iWSA-masks in native space.

Statistical analysis

The mean values of each hemodynamic parameter were calculated separately for hemispheres ipsilateral and contralateral to the stenosis inside and outside the iWSAs with additional GM (iWSA-GM) and WM (iWSA-WM) masks for each participant. Two evaluations were conducted on a group level. First, the average values of each parameter within the iWSA were compared using paired-scatter plots between both hemispheres. This was done separately for ICAS-patients and HCs. Absolute parameter values per hemisphere were compared between ICAS-patients and HCs. Second, the parameter lateralization between hemispheres was compared inside vs. outside iWSAs for GM and WM of ICAS-patients. For comparisons between hemispheres, one-sample t-tests were applied. For comparisons between groups, two-sample t-tests were applied. Generally, values of $p < 0.05$ were considered statistically significant.

Results

Figure 2 shows exemplary data of two ICAS-patients. These results demonstrate impairment of multiple hemodynamic parameters. Specifically, CBF and CVR were decreased ipsilaterally to the stenosis and there was concomitant elevation of rCBV, OEC and CTH. The location and strength of the

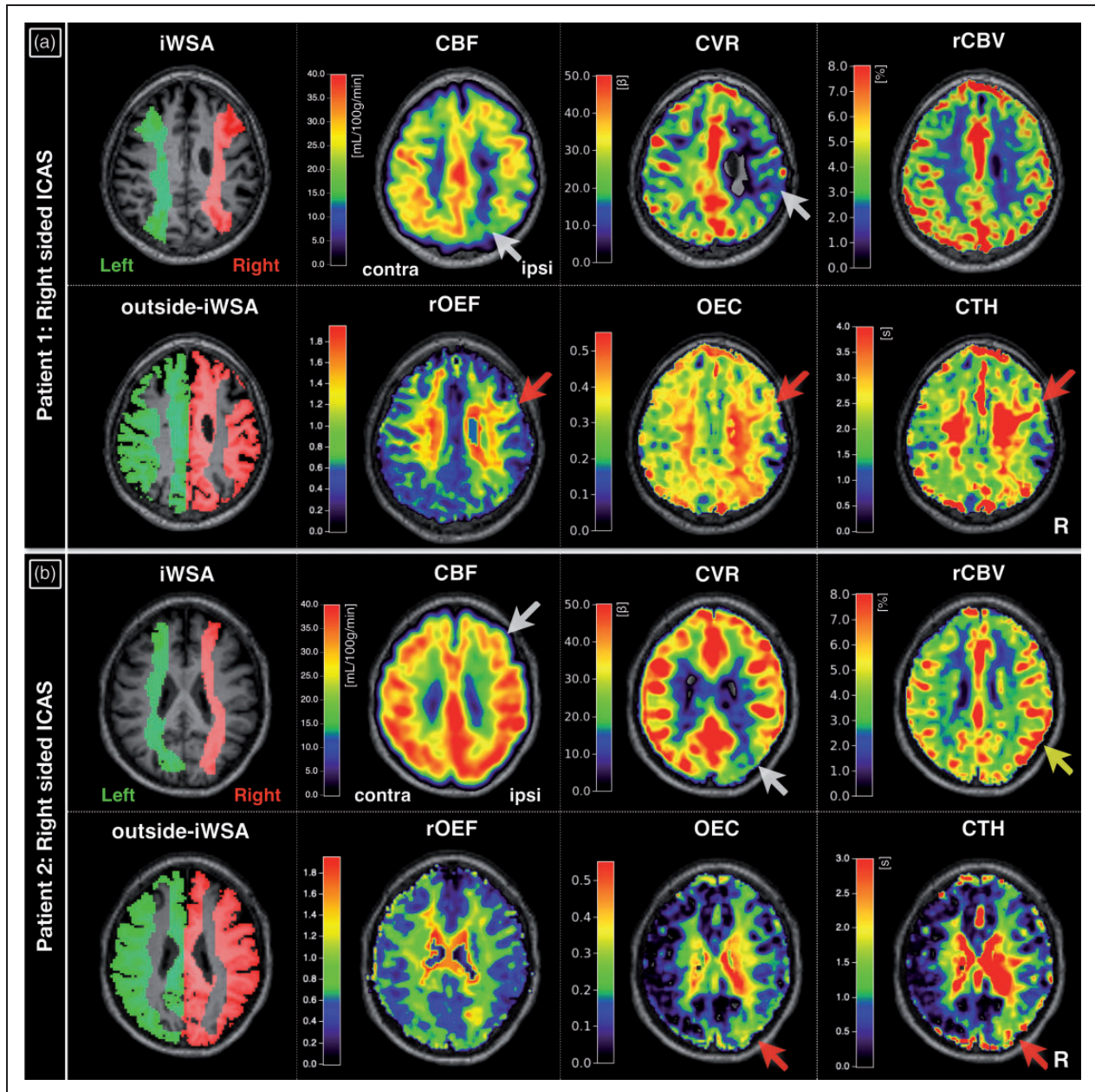


Figure 2. Exemplary parameter maps of two patients with right-sided ICAS. Hemodynamic parameter maps show individually defined watershed areas (iWSA), CBF, CVR, rCBV, brain regions complementary to iWSAs (outside-iWSA), rOEF, OEC and CTH. CBF and CVR were decreased ipsilateral to the stenosis in both patients (white arrows, a, b). In the first patient, focal ipsilateral rOEF increases correspond to elevated OEC and CTH (red arrows, a). In the second patient, rCBV was ipsilaterally increased (yellow arrow, b). Generally, OEC and CTH elevations appear spatially more expanded (red arrows, a, b). For group analyses, each hemisphere's subject-specific iWSA and outside-iWSA masks with additional GM/WM-masking were applied to parameter maps and average values calculated within each volume of interest (VOI). iWSA: individual watershed areas; CBF: cerebral blood flow; CVR: cerebrovascular reactivity; rCBV: relative cerebral blood volume; rOEF: relative oxygen extraction fraction; OEC: oxygen extraction capacity; CTH: capillary transit-time heterogeneity.

impairments was variable for the six parameters, e.g. regions of obvious CBF and rCBV impairments did not overlap in the second patient (Figure 2(b)). Furthermore, the first patient had much more widespread CVR decreases, but no

apparent rCBV effects in the displayed slice (Figure 2 (a)). Minor focal rOEF increases were only observed in the first patient, and they corresponded to elevated OEC and CTH, which appeared to be spatially more extended.

Group level comparisons between hemispheres in ICAS-patients showed statistically significant lateralization of all evaluated parameters ($p < 0.01$), except for rOEF (Figures 3 and 4). Those lateralization of CBF, CVR, rCBV, OEC and CTH in ICAS-patients were significantly different from HCs ($p < 0.05$). In HCs, all parameters were symmetrical between hemispheres. Although OEC showed significant side differences in HCs ($p < 0.001$), the magnitude of differences was negligible (OEC = 0.38 in both hemispheres within iWSA-GM, Table 2). In the patients, CBF was decreased in the hemisphere ipsilateral to the stenosis (lateralization Δ CBF = -18% in iWSA-GM, $p < 0.001$, Figure 3). Absolute CBF values in the contralateral ICAS hemisphere were comparable to HCs (CBF in iWSA-GM ≈ 30 ml/100g/min). For CVR, beta-values were statistically significantly decreased ipsilateral to

the stenosis (-15% in iWSA-GM, $p < 0.001$). Contralateral CVR values in GM were decreased compared to HCs, while contralateral CVR values in WM were comparable to HCs. Relative CBV was significantly increased in the ipsilateral ICAS hemisphere compared to the contralateral hemisphere (+5% in iWSA-GM, $p < 0.01$). Values of rCBV in the contralateral ICAS hemispheres were comparable to HCs within WM, while rCBV in GM was decreased in both ICAS hemispheres compared to HCs. Analysis of rOEF revealed symmetry between hemispheres with comparable values to HCs (rOEF ≈ 0.6 in iWSA-GM, Figure 4). Only the variability of rOEF was increased across ICAS-patients (bilaterally increased standard deviation (SD) by +50% compared to HCs within iWSA-GM, Table 2). Values of OEC and CTH were ipsilaterally increased (OEC by +12% and CTH by

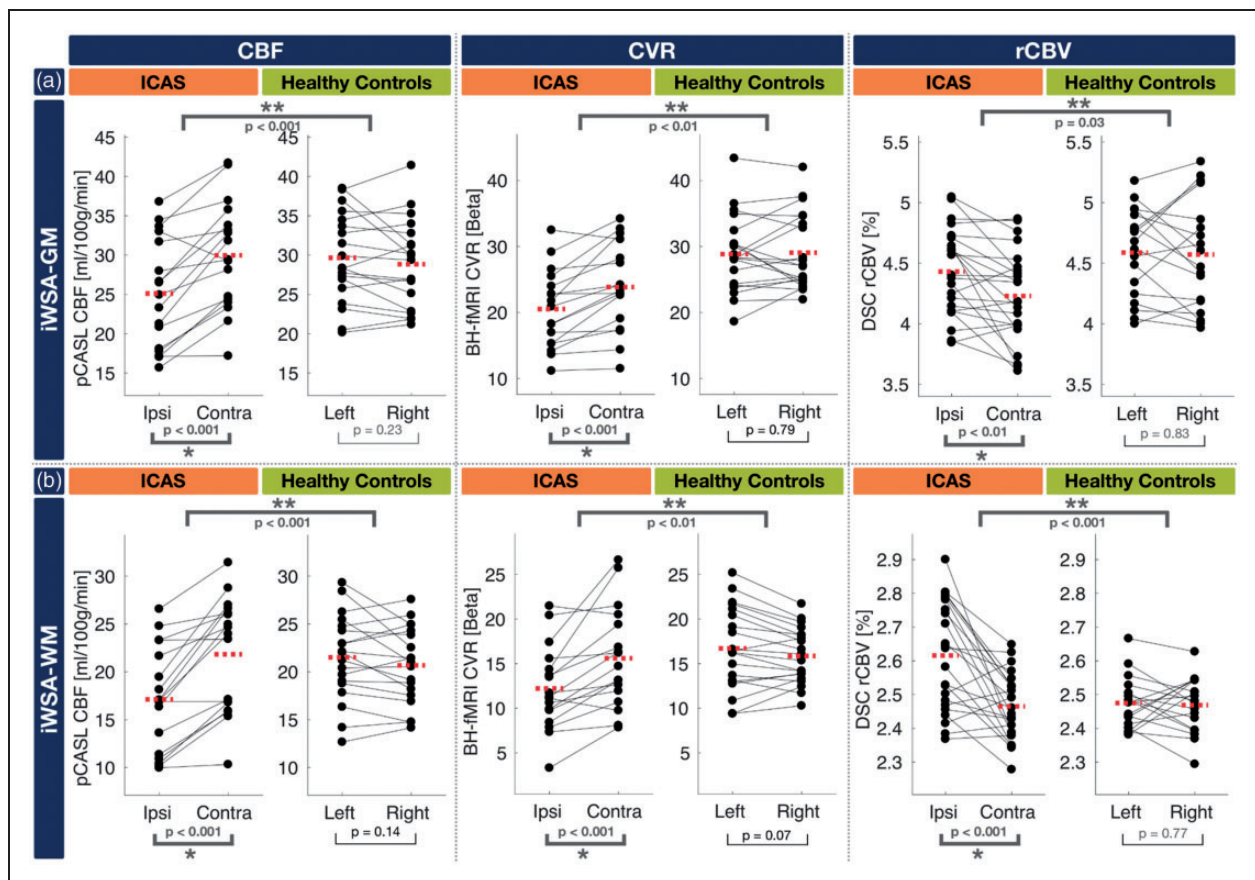


Figure 3. Paired scatterplots comparing perfusion-related parameters between hemispheres within iWSAs in GM (a) and WM (b). CBF, CVR, and rCBV are compared for ICAS patients and healthy controls. To facilitate direct comparisons, scatterplots of parameter values in GM and WM of iWSAs are stacked in (a) and (b). Dots represent the mean parameter values of each subject within iWSAs in GM or WM – lines connect the mean values of both hemispheres from the same subjects. Dashed red lines indicate parameter's group mean values within each hemisphere. In ICAS patients, all parameters showed statistically significant differences between hemispheres (one-sample t-test, $p < 0.05$, asterisks) and lateralization was also significantly different from HCs (two-sample t-test, $p < 0.05$, double asterisks). All parameters were symmetrical between the hemispheres of HCs. ICAS: internal carotid artery stenosis; CBF: cerebral blood flow; CVR: cerebrovascular reactivity; rCBV: relative cerebral blood volume; iWSA: individual watershed areas.

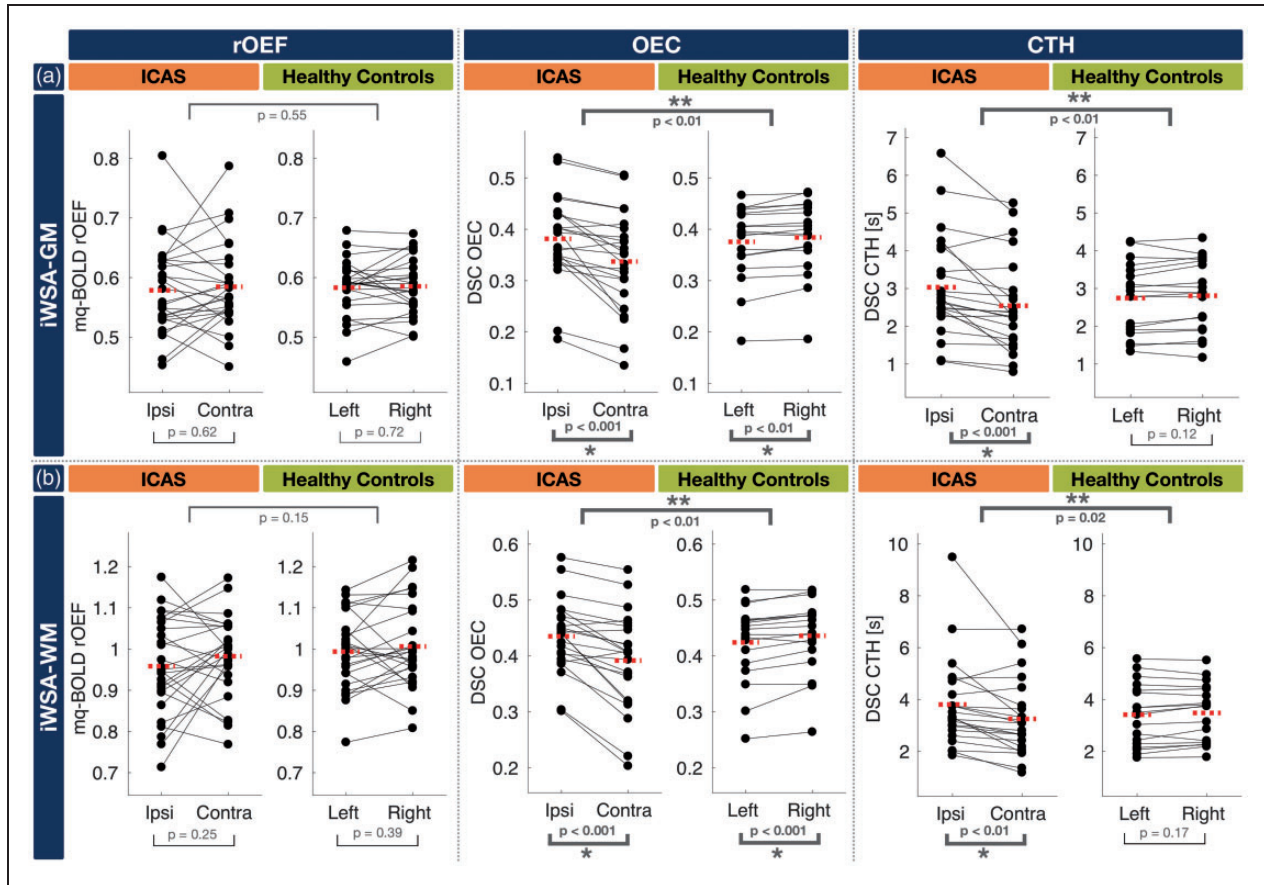


Figure 4. Paired scatterplots comparing oxygenation-related parameters between hemispheres within iWSAs in GM (a) and WM (b). rOEF, OEC and CTH are compared for ICAS patients and healthy controls. To facilitate direct comparisons, scatterplots of parameter values in GM and WM are stacked in (a) and (b). Dots represent mean parameter values of each subject within iWSA in GM or WM – lines connect mean values of both hemispheres from the same subjects. Dashed red lines indicate parameter's group mean values within each hemisphere. In ICAS patients, all parameters except rOEF showed statistically significant differences between hemispheres (one-sample t-test, $p < 0.05$, asterisks) and lateralization was also significantly different from HCs (two-sample t-test, $p < 0.05$, double asterisks). Although OEC showed significant side differences in HCs, the magnitude of differences was negligible. All parameters were symmetrical between the hemispheres of HCs. rOEF: relative oxygen extraction fraction; OEC: oxygen extraction capacity; CTH: capillary transit-time heterogeneity; iWSA: individual watershed areas; ICAS: internal carotid artery stenosis.

+18% within iWSA-GM, $p < 0.001$, Figure 4). Furthermore, the CTH variability was increased (SD by +41% in ipsilateral iWSA-GM compared to HCs, Table 2). All average hemisphere's parameter values are summarized in Table 2.

Parameter lateralization in ICAS-patients was compared inside vs. outside iWSAs and separately masked with GM and WM (Figure 5(a) and (b), respectively). Generally, CBF, CVR and rCBV showed stronger lateralization inside iWSAs compared to outside iWSAs. In detail, CBF and CVR were significantly lateralized in all masks, inside as well as outside of iWSA-GM and iWSA-WM ($p < 0.01$). Despite CBF and CVR lateralization outside iWSAs, the effects inside iWSAs were still significantly stronger (+117% for ΔCVR inside vs. outside iWSA-GM, $p < 0.01$). Additionally, the effects

in WM were stronger (Figure 5(b)) compared to GM (Figure 5(a)). For example, lateralization of CBF and CVR was stronger within iWSA-WM ($\Delta\text{CBF} = \Delta\text{CVR} = -24\%$) versus iWSA-GM ($\Delta\text{CBF} = -18\%$ and $\Delta\text{CVR} = -15\%$). The effects of ΔrCBV were similar to ΔCBF and ΔCVR but had the opposite sign. Relative CBV was also significantly lateralized outside iWSAs but was significantly stronger affected inside iWSA-WM (+96% for ΔrCBV iWSA-WM inside vs. outside, $p = 0.016$) and with a strong trend for iWSA-GM (+56%, $p = 0.058$). Nevertheless, lateralization of rCBV was weaker compared to CBF or CVR ($\Delta\text{rCBV} = 6\%$ vs. $\Delta\text{CBF} = \Delta\text{CVR} = -24\%$ within iWSA-WM). Regarding OEC and CTH, lateralization was observed in all masks, specifically inside/outside iWSA-GM/WM (10% to 18%). Contrary to the

Table 2. Average hemodynamic parameter values inside GM and WM of iWSAs.

Mask	Group	Hemisphere	Hemodynamic parameters					
			CBF (ml/100g/min)	CVR (Beta)	rCBV (%)	rOEF	OEC	CTH (s)
iWSA-GM	Healthy	Left	29.7 ± 5.7	28.9 ± 5.8	4.59 ± 0.37	0.58 ± 0.05	0.38 ± 0.07 *	2.75 ± 0.95
		Right	28.8 ± 5.6	29.1 ± 5.8	4.57 ± 0.45	0.59 ± 0.05	0.38 ± 0.07 *	2.81 ± 0.95
	ICAS	Ipsi	25.1 ± 6.9 *	20.5 ± 5.9 *	4.43 ± 0.36 *	0.58 ± 0.08	0.38 ± 0.08 *	3.03 ± 1.34 *
		Contra	30.0 ± 6.9 *	23.8 ± 6.6 *	4.23 ± 0.38 *	0.59 ± 0.07	0.34 ± 0.10 *	2.54 ± 1.23 *
iWSA-WM	Healthy	Left	21.5 ± 4.5	16.7 ± 4.6	2.48 ± 0.08	0.99 ± 0.09	0.42 ± 0.07 *	3.42 ± 1.20
		Right	20.7 ± 4.0	15.9 ± 3.1	2.47 ± 0.08	1.01 ± 0.10	0.44 ± 0.07 *	3.48 ± 1.11
	ICAS	Ipsi	17.1 ± 5.5 *	12.2 ± 3.1 *	2.62 ± 0.16 *	0.96 ± 0.12	0.44 ± 0.07 *	3.81 ± 1.70 *
		Contra	21.8 ± 6.0 *	15.6 ± 5.6 *	2.47 ± 0.10 *	0.98 ± 0.10	0.39 ± 0.09 *	3.25 ± 1.44 *

Note: Hemodynamic parameters CBF, CVR, rCBV, rOEF, OEC and CTH were evaluated inside masks of iWSA in GM and WM for healthy controls and ICAS patients, and comparisons were made between both hemispheres. For healthy controls, left vs. right hemispheres were compared and for ICAS patients between hemispheres ipsilateral vs. contralateral to the stenosis (mean ± standard deviation). Statistically significant differences based on t-tests between hemispheres are indicated by asterisks.

CBF: cerebral blood flow; CVR: cerebrovascular reactivity; rCBV: relative cerebral blood volume; rOEF: relative oxygen extraction fraction; OEC: oxygen extraction capacity; CTH: capillary transit-time heterogeneity iWSA: individual watershed areas; ICAS: internal carotid artery stenosis.

previously reported parameters, OEC and CTH were similarly affected inside and outside iWSAs. In addition, Δ OEC and Δ CTH lateralization was comparable in GM (Figure 5(a)) and WM (Figure 5(b)).

Discussion

In this study, we present a multimodal MRI-based investigation of hemodynamic impairments in unilateral ICAS. Specifically, we explored whether six perfusion and oxygenation sensitive parameters were affected more inside vs. outside iWSAs. CBF was measured with a single-PLD pCASL, CVR by breath-hold fMRI (BH-fMRI), rCBV by DSC, rOEF by mq-BOLD and OEC as well as CTH by parametric modeling of DSC-data. Individual WSAs were defined semi-automatically using DSC-based TTP maps.

We showed impairments of CBF, CVR, rCBV, OEC and CTH – but not of rOEF – in unilateral ICAS-patients. We also showed that all parameters were unaffected in our healthy control cohort, which affirmed the specificity of the selected parameters. According to our hypothesis, impairments of CBF, CVR and rCBV in ICAS were more pronounced inside iWSAs than outside. In addition, impairments were stronger in WM compared to GM. At the same time, OEC and CTH were severely impaired, but independent of iWSA locations. Measured impairments of the individual parameter values were in agreement with previously reported literature values. Beyond that, comparisons of complex multimodal parameter alterations offer a broader perspective on the pathophysiological conditions of complex microvascular impairments in ICAS, which is discussed below.

Impaired perfusion (CBF, CVR and rCBV)

Ipsilateral to the stenosis, we measured decreased CBF (–18% in iWSA-GM), which is in agreement with previous PET⁵² and MRI studies^{7,53} as well as the model of Powers et al.¹⁸ In the contralateral hemisphere, absolute CBF values were comparable to HCs, but the variability was increased (SD across subjects increased by +22% in patients compared to HCs within iWSA-GM). This could be explained by subject specific collateralizations of blood flow,¹⁵ that affect the contralateral hemisphere, and thereby increasing the inter-subject variability of contralateral CBF. Even though no obvious signs of arterial delay artefacts were found, CBF in watershed areas of ICAS-patients may potentially be affected by delayed blood arrival.^{54–58}

We detected decreased CVR on the side of the stenosis in ICAS-patients (–15% compared with contralateral values and –29% compared with HCs in iWSA-GM), as predicted by the basic hemodynamic model and in agreement with other studies.^{5,24} We also found decreased CVR in the contralateral hemisphere (–18% compared with HCs in iWSA-GM). This can be explained by blood flow collateralization from the contralateral side, which caused hemodynamic stress even in the contralateral hemisphere. Those observed bilateral effects have been described previously⁵⁹ and highlight the fact that unilateral ICAS can affect both hemispheres. Nevertheless, CVR on a group level was still significantly lateralized between the hemispheres (Δ CVR = –24% in iWSA-WM), which underlines the high sensitivity of hemispheric CVR comparisons.

We also found lateralization of rCBV with higher values ipsilateral to the stenosis (+5% in iWSA-GM),

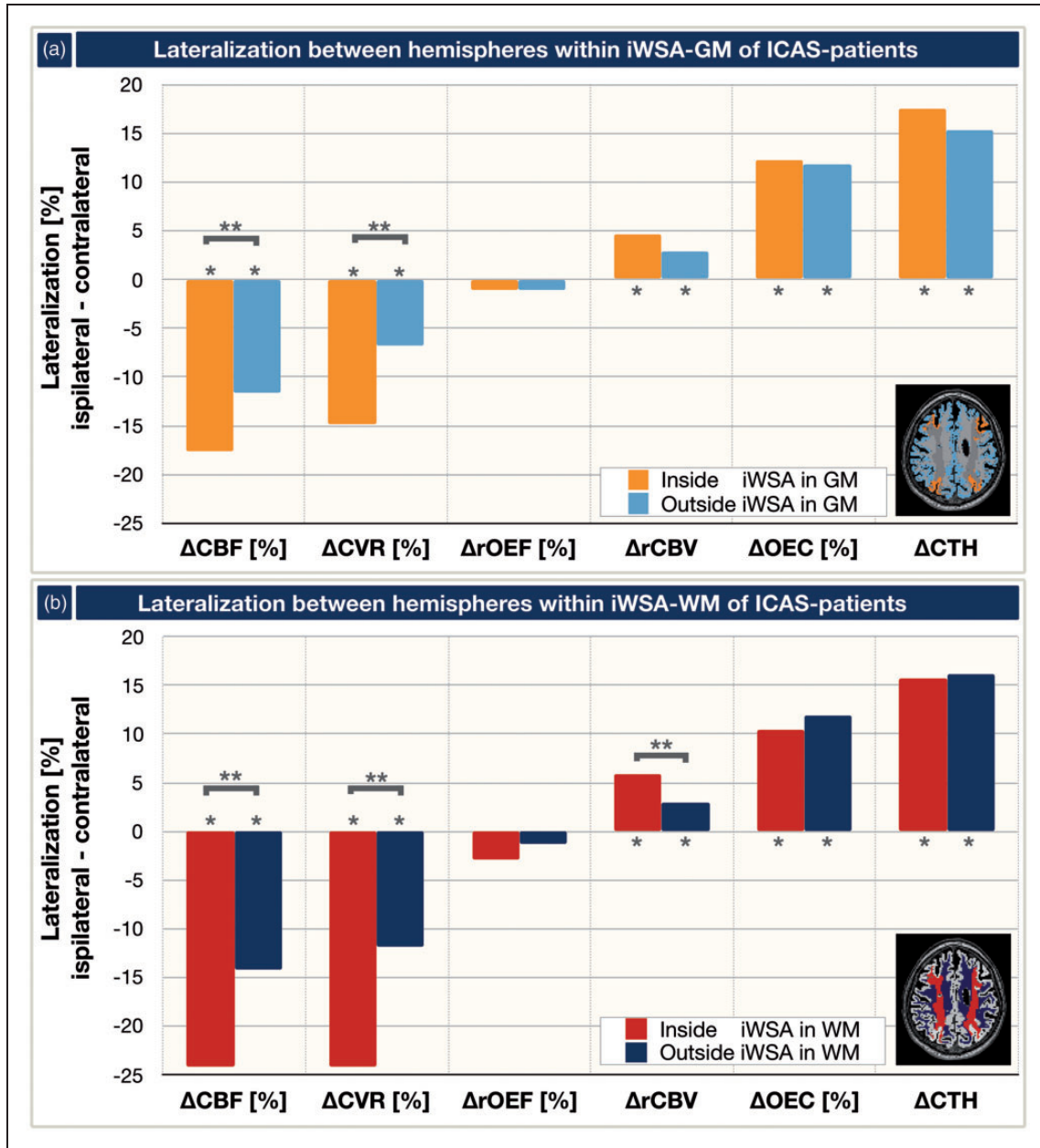


Figure 5. Parameter's lateralization between hemispheres inside vs. outside of iWSAs in GM (a) and WM (b). Lateralization was calculated from differences of mean values between hemispheres ipsilateral and contralateral to the stenosis. Four VOIs were compared (see exemplary inlays): inside iWSAs in GM (orange, a), outside iWSAs in GM (light blue, a), inside iWSAs in WM (red, b) and outside iWSAs in WM (dark blue, b). Negative Δ CBF and Δ CVR corresponded to decreased values ipsilateral to the stenosis, while Δ rOEF was unaffected and Δ rCBV, Δ OEC and Δ CTH were increased. Asterisks indicate statistically significant lateralization (one-sample t-test, $p < 0.01$). ICAS-related impairments of Δ CBF, Δ CVR and Δ rCBV were statistically significantly enhanced inside of iWSAs compared to the outside of iWSAs (double asterisks, one-sample t-test, $p < 0.05$).

CBF: cerebral blood flow; CVR: cerebrovascular reactivity; rCBV: relative cerebral blood volume; OEC: oxygen extraction capacity; CTH: capillary transit-time heterogeneity.

which was expected from the model and also agrees with previous publications.^{18,52,53,60,61} Ipsilateral rCBV increases alongside with decreased CVR, which confirmed the assumed chronic vasodilation.⁶² However, we also observed bilateral effects. Values of

rCBV within iWSA-GM in both hemispheres were generally lower for ICAS-patients compared to HCs, which is in excellent agreement with previous PET measurements.⁶⁰ Within iWSA-WM masks, rCBV was comparable in contralateral ICAS hemispheres

and HCs ($\approx 2.5\%$, Table 2), due to our processing with rCBV normalization to 2.5% in NAWM.^{27,51}

Spatial variability of perfusion impairments

Interestingly, the localizations of CBF, CVR, and rCBV impairment were highly variable among patients. In addition, the spatial overlap of compromised hemodynamic biomarkers within the same subject was highly variable. These effects clearly demonstrate the limitation of the simplified model that was proposed by Powers et al.¹⁸ on a single subject level. It furthermore demonstrated that the evaluated parameters indeed yielded complementary information (see Supplemental Figure 1) about different pathophysiological effects. For example, the ICAS patient presented in Figure 2(a) showed spatially non-congruent impairments of CBF and CVR without obvious rCBV effects. In contrast, the second patient shown in Figure 2(b) demonstrated rCBV and CVR effects at very similar locations, while CBF was impaired in other regions. We assume two major causes for this high inter-subject spatial variability. First, the varying degrees of the stenosis ($81.2 \pm 10.1\%$, Table 1) influenced the CPP decreases and this explains inter-subject variations of hemodynamic impairments. Second, configurations of the circle of Willis can vary a great deal among patients and can cause very different collateralization patterns.^{15,63} An unilateral CPP decrease in ICAS together with high recruitment of collateral blood flow can cause strong shifts of perfusion territories in the entire brain.^{14,63} Consequently, locations of hemodynamic impairments are highly subject specific. At the same time, different hemodynamic mechanisms are indicated to act at different locations, which complicated the interpretation of individual maps of hemodynamic biomarkers. Therefore, our proposed protocol for measurements of multiple hemodynamic biomarkers within a single imaging session is a promising method that can help to better explain highly subject specific impairments. Additionally, evaluation within iWSAs indeed helps to overcome the disturbing effects of the high spatial variability, as iWSAs specifically select the most severely impaired areas of CBF, CVR and rCBV at the same time, as initially hypothesized.

The perfusion impairments of CBF, CVR and rCBV were found to be enhanced in WM compared to GM of iWSAs. The stronger lateralization of Δ CBF and Δ rCBV in unilateral ICAS within WM agreed with results from a previous study.⁶¹ Physiologically, the stronger effects within WM-iWSAs can be well explained by the architecture of the blood supply to GM and WM.¹³ Sections of iWSAs in WM are expected to be located at the most distal arterial

branches, where CPP is generally assumed to be the lowest. Additional influencing factors may also be due to delay effects in single-PLD pCASL^{54–56} and delay effects in CVR-imaging.⁶⁴ Even though CBF evaluation by ASL is known to be challenging in WM due to a lower SNR²³ and partial volume effects,⁶⁵ a previous study showed its sensitivity to WM perfusion deficits,⁶⁶ which was also supported by our successful evaluations on a group level. Overall, our measured impairments of CBF, CVR and rCBV in WM are consistent with previous reports in the literature⁶¹ and indicate the highest sensitivity to hemodynamic impairments within WM of iWSAs.

Oxygenation

In contrast to the previously discussed perfusion parameters, average rOEF values by mq-BOLD were found to be unaffected in ICAS-patients. On a group level, we neither found lateralization between hemispheres nor significant differences between ICAS-patients and the HC-group. This finding of an unaffected rOEF with concomitant ipsilateral CBF decreases was in excellent agreement with a recent study from Bouvier et al. using a very similar methodology.⁷ Using the model of Power et al.,¹⁸ these results implied that high-grade asymptomatic ICAS-patients are not yet in the range of misery perfusion.⁶⁷ Nevertheless, individual patients showed slight focal increases of rOEF, which probably contributed to the observed increase in rOEF variability in ICAS-patients within both hemispheres (bilateral SD increased by +50% in ICAS compared to HCs within iWSA-GM, Table 2). This is in agreement with a PET study, that demonstrated bilateral increases of OEF variability in ICAS-patients compared to controls.⁶⁰

According to Power's model,¹⁸ which is based on Fick's principle in an iso-metabolic state,⁶⁸ rOEF should increase in regions of reduced CBF to maintain the oxidative metabolism. An explanation for this apparent mismatch of reduced CBF and unchanged rOEF might be subtle damage to the neuronal tissue due to previous, temporary lapses in oxygen, which agrees with the subtle cognitive impairments detected in our study cohort.² Another possibility is that additional factors regulate the cerebral oxygen delivery as proposed by Hyder et al.^{20–22} Their model permits changes in oxygen diffusivity at the capillary level due to changes in perfusion and also related alterations in rheological parameters at the microscopic level. Tube hematocrit, defined as the instantaneous volume fraction of red blood cells (RBCs) in a capillary, may change dynamically as the velocities of RBCs and plasma in capillaries are not equivalent. Tube hematocrit is uniquely different from discharge hematocrit,

which is a measure of volume percentage of RBCs in blood and consistently approximates systemic hematocrit values. Thus, differences between tube and discharge hematocrit could explain our results and this could also explain the variability in local regulation observed across our subjects.⁶⁹ Alternatively, variations in oxygen diffusivity may also have an association with the above discussed increased rOEF variability, i.e. oxygen diffusivity might be more severely altered in some patients. Thus, direct MRI-based measurements of oxygen diffusivity would be highly promising to better understand the complexities of cerebral oxygen delivery.

Germuska et al. recently proposed an interesting technique for modeling oxygen diffusivity based on MRI measurements during gas challenges.⁷⁰ However, their combination of competing models, namely where oxygen diffusion is either limited⁷¹ or not,²⁰ requires further research. Oxygen diffusivity at the systemic level is determined by the discharge hematocrit. As correlations between high blood pressure and elevated discharge (or systemic) hematocrit have been demonstrated^{72,73} and many of our ICAS-patients showed hypertension (79%, see Table 1), the systemic hematocrit level of our patients might be elevated. Following this argumentation, the higher blood pressure in ICAS could be potentially linked to a higher variability in oxygen diffusivity and thus increased rOEF variability. However, since we did not measure hematocrit levels in our participants, future studies evaluating hematocrit levels are clearly required to further evaluate this hypothesis.

Capillary transit time heterogeneity and dysfunction

Based on parametric modeling of DSC-data, we observed increased capillary transit-time heterogeneity on the side of the stenosis, which was in accordance with a previous study in ICAS-patients.³⁰ Interestingly – and unlike previously discussed for CBF, CVR and rCBV – we found that CTH lateralization was independent of iWSA locations. These CTH impairments beyond iWSAs are in agreement with a recent study that demonstrated a spatial mismatch of CTH and T_{\max} impairments.³⁰ Since T_{\max} is closely related to TTP, which was used to delineate our iWSAs,¹⁴ our finding of mismatching CTH impairments and iWSA regions excellently agreed with their findings. A possible physiological explanation might be that TTP is more sensitive to macrovascular perfusion,⁷⁴ while CTH is assumed to be particularly sensitive to capillary flow.³⁰

Lateralization of CTH outside-iWSA was stronger than for any other parameter ($\approx 16\%$ outside iWSAs). This result points to a more widespread microvascular

pathology beyond areas that are obviously affected by perfusion deficits. It is, therefore, possible that CTH offers complementary information about microscopic rheological events of capillary hemodynamics compared to CBF, CVR and rCBV, as these behave fundamentally differently inside and outside of iWSAs. Consequently, CTH is a promising early indicator of microvascular impairments in ICAS with rather subtle CPP decreases. At the same time, CTH may detect spatially more widespread microvascular involvement compared to CBF, CVR or rCBV. As DSC-imaging could be applied in standard clinical diagnostic MRI of ICAS in the future,⁷⁵ additional promising information could be gathered by parametric modeling with respect to CTH.

Furthermore, there might be a link between CTH and the previously discussed oxygen diffusivity. As most oxygen diffusion through the vessel walls is expected to come from the capillaries,⁷⁶ capillary flow patterns have also been linked with the efficacy of oxygen extraction.⁵³ Thus, variations in the oxygen diffusivity may be potentially moderated by CTH.^{28,77} Along this line, in 2012, Jespersen and Østergaard proposed to additionally derive information on tissue oxygen supply via parametric modeling of DSC-data.²⁸ They claimed that CTH increases would at some point result in a decrease of OEC, a condition they termed ‘malignant’ CTH. Following their argumentation, ICAS-patients in our cohort would still reside in the regime of benign CTH with rather increased OEC, which agrees with our observations. With respect to a rather qualitative interpretation, exemplary parameter maps imply some congruency of spatial patterns between OEC and CTH maps in our subjects. Furthermore, lateralization of Δ OEC and Δ CTH was similar on a group level (Figure 4) and also among individual ICAS-patients (see Supplemental Figure 1). Thus, a mild to moderate vascular pathology is implied in our patients with reduced perfusion pressure and capillary constrictions, but rather no capillary occlusions, according to previously presented simulations.⁷⁸ However, the exact physiological interpretation of OEC is difficult because it relies on the validity of a complex modeling approach, which requires further investigation. Even though OEC and rOEF are both supposed to be related to cerebral oxygenation, average OEC and rOEF values did not correlate within iWSAs (see Supplemental Figure 2). This is certainly due to the fact that they rely on different models as introduced in the methods (see ‘Image analysis’ section in the methods description).

Applicability and Limitations

This study has several strengths, but also some limitations. An obvious strength is the simultaneous multimodal assessment of cerebral perfusion and

oxygenation parameters, which allows the evaluation of specific stenosis-related hemodynamic effects within subjects. Given the high variability of the hemodynamic situation in individual patients (see Supplemental Figure 1), multimodal MRI is especially promising to evaluate subject specific impairments.

Regarding the different applied methods, CBF imaging by pCASL is a very promising non-invasive method for initial non-invasive diagnostics.²³ However, it is not applicable after stenting, because of SAR limitations. We sought to minimize potential delay effects of single-PLD pCASL by using longer PLDs, as suggested by the consensus recommendations.²³ Those delay effects are a generally known methodological issue of single-PLD pCASL.^{54–56} We did not observe obvious signs of major delays in the label arrival by visual and quantitative inspection of our data. However, quantitative errors in the regions with potentially prolonged longer ATT, such as the watershed areas, cannot completely be excluded.^{57,58} To address this issue in the future, time-encoded ASL could be applied.^{79,80} Generally, measured CBF was lower than expected, which has been observed before with this dataset¹¹ and can be explained by the applied BGS.^{40,41}

Breath-hold fMRI for CVR imaging is sensitive to impairments in ICAS, non-invasive, easy to apply, and applicable after stenting. Although our implementation of BH-fMRI was limited by use of comparably short CO₂ stimuli and unknown end-tidal CO₂ concentrations,²⁴ the applied scheme using 15 second breath-holds already demonstrated good reproducibility⁸¹ and was found to be adequate for relative CVR comparisons.²⁴ To further increase the reliability, we performed a comprehensive analysis applying a respiratory response function.⁴³ Theoretically, motor cortex activation may cause minor bilateral effects. As an alternative, gas challenges could be applied that would be more precise, but also more complicated.²⁴ Using gas challenges, additional voxel-wise delay information can be derived, which already showed promising results in Moyamoya patients.⁸²

DSC imaging offers a broad range of different parameters and promising information about capillary dysfunction when using parametric modeling. However, the currently ongoing discussion about contrast agent accumulations should be considered.⁸³

Measurements of rOEF by mq-BOLD did not show direct benefits for diagnostic evaluation of our high-grade, asymptomatic ICAS-patients. Nevertheless, research studies can benefit from concomitant rOEF and CBF measurements when investigating the oxygen metabolism.¹¹ Despite the known systematic rOEF elevations in mq-BOLD^{27,84} and neglect of intravascular signal contributions as well as vessel size

dependent hematocrit variations, this method has been successfully applied in studies on different brain pathologies and compares well with PET measurements.^{11,27,49,85–87} Furthermore, improved quantitative T₂ mapping by a 3D GraSE sequence significantly reduces rOEF values toward lower, physiologically more realistic values.⁸⁴ This is a viable alternative for future studies. The application of mq-BOLD in WM could be considered another potential limitation, as the underlying model assumes randomly oriented blood vessels.⁴⁸ Although vessel orientation effects in WM have been observed,⁸⁸ recently, reasonably low orientation-related errors of mq-BOLD were demonstrated in WM.⁸⁹

Future multi-center studies – such as the CREST-H study⁷⁵ – are clearly necessary to further resolve current limitations and to gain an even deeper understanding of the hemodynamic impairments in ICAS. Finally, improvement in the treatment guidelines could be achieved by considering perfusion and oxygen sensitive biomarkers. In addition to possible future applications in ICAS, the proposed MRI protocol is also highly promising for application in other cerebrovascular diseases (CVD), which are often also associated with elevated stroke risks.⁵

Conclusion

In the presented study, we demonstrated the sensitivity of our multimodal MRI protocol to detect hemodynamic impairments in unilateral ICAS. Hemodynamic parameters were found to be clearly lateralized between hemispheres in ICAS-patients, whereas in HCs, all parameters were symmetrical between the hemispheres affirming specificity. As hypothesized, the most pronounced changes of CBF, CVR and rCBV in ICAS-patients were detected within iWSAs. Contrary to simple models, we found subject-specific impairments of the investigated six parameters CBF, CVR, rCBV, rOEF, CTH, and OEC, which demonstrated their ability to yield complementary information about the underlying pathology. We also found contralateral effects in some patients, which can be explained by collateral flow. Interestingly, CTH and OEC increases were independent of iWSA locations, which indicated more widespread impairments of capillary function. Our results offer substantial improvement in understanding the relationship of involved parameters in individual patients. Therefore, multimodal MRI is highly promising to improve clinical diagnostics of asymptomatic ICAS by accounting for individual hemodynamic impairments towards personalized stroke risk assessment. Most importantly, application of iWSAs increased the sensitivity for impairments of CBF, CVR and rCBV. Thus, knowledge about iWSA

locations can even facilitate detection of subtle hemodynamic changes using standard MRI protocols.

Funding

The author(s) disclosed receipt of the following financial support for the research, authorship, and/or publication of this article: This work was supported by the Friedrich-Ebert-Stiftung (grant to SK), the Dr.-Ing. Leonhard Lorenz-Stiftung (grant to SK: 971/19 and JG: 915/15), by the Faculty of Medicine of the Technical University of Munich (grant to JG: KKF E12) and the German Research Foundation (DFG) – Project number PR 1039/6-1 (grant to CP). FH was supported by NIH grants (R01 MH-067528, R01 NS-100106).

Acknowledgements

We thank Michael Kallmayer and Hans-Henning Eckstein for their support in the patient recruitment (both from TUM) as well as Kim van de Ven (Philips Healthcare, Best, Netherlands) and Hendrik Kooijman (Philips Healthcare, Hamburg, Germany) for their support with the ASL imaging.






Authors' contributions

SK: study design, data acquisition, data analysis, interpretation of the results, article writing; JG: study design, data acquisition, interpretation of the results, article editing; JP: data analysis, interpretation of the results, article editing; MBH: data analysis, interpretation of the results, article editing; KM: interpretation of the results, proofreading; CZ: study design, proofreading; FH: interpretation of the results, article editing; CP: study design, study supervision, interpretation of the results, article editing.

Declaration of conflicting interests

The author(s) declared no potential conflicts of interest with respect to the research, authorship, and/or publication of this article.

ORCID iDs

Stephan Kaczmarz  <https://orcid.org/0000-0001-7694-7012>
 Jens Göttler  <https://orcid.org/0000-0002-5746-2156>
 Jan Petr  <https://orcid.org/0000-0002-3201-6002>
 Mikkel Bo Hansen  <https://orcid.org/0000-0002-8619-1519>
 Christine Preibisch  <https://orcid.org/0000-0003-4067-1928>

Supplemental material

Supplemental material for this article is available online.

References

1. Petty GW, Brown RD Jr, Whisnant JP, et al. Ischemic stroke subtypes: a population-based study of incidence and risk factors. *Stroke* 1999; 30: 2513–2516.
2. Gottler J, Kaczmarz S, Nuttall R, et al. The stronger one-sided relative hypoperfusion, the more pronounced ipsilateral spatial attentional bias in patients with asymptomatic carotid stenosis. *J Cereb Blood Flow Metab* 2020; 40: 314–327.
3. Norling AM, Marshall RS, Pavol MA, et al. Is hemispheric hypoperfusion a treatable cause of cognitive impairment? *Curr Cardiol Rep* 2019; 21: 4.
4. Bond R, Rerkasem K and Rothwell PM. Systematic review of the risks of carotid endarterectomy in relation to the clinical indication for and timing of surgery. *Stroke* 2003; 34: 2290–2301.
5. Donahue MJ, Achten E, Cogswell PM, et al. Consensus statement on current and emerging methods for the diagnosis and evaluation of cerebrovascular disease. *J Cereb Blood Flow Metab* 2018; 38: 1391–1417.
6. Jalbert JJ, Nguyen LL, Gerhard-Herman MD and et al. Outcomes after carotid artery stenting in Medicare beneficiaries, 2005 to 2009. *JAMA Neurol* 2015; 72: 276–286.
7. Bouvier J, Detante O, Tahon F, et al. Reduced CMRO2 and cerebrovascular reserve in patients with severe intracranial arterial stenosis: a combined multiparametric qBOLD oxygenation and BOLD fMRI study. *Hum Brain Mapp* 2015; 36: 695–706.
8. Donahue MJ, van Laar PJ, van Zijl PCM, et al. Vascular space occupancy (VASO) cerebral blood volume weighted MRI identifies hemodynamic impairment in patients with carotid artery disease. *J Magn Reson Imag* 2009; 29: 718–724.
9. Vakil P, Lee JJ, Mouannes-Srouf JJ, et al. Cerebrovascular occlusive disease: quantitative cerebral blood flow using dynamic susceptibility contrast MR imaging correlates with quantitative H2[15O] PET. *Radiology* 2013; 266: 879–886.
10. Derdeyn CP, Videen TO, Yundt KD, et al. Variability of cerebral blood volume and oxygen extraction: stages of cerebral haemodynamic impairment revisited. *Brain* 2002; 125: 595–607.
11. Gottler J, Kaczmarz S, Kallmayer M, et al. Flow-metabolism uncoupling in patients with asymptomatic unilateral carotid artery stenosis assessed by multi-modal magnetic resonance imaging. *J Cereb Blood Flow Metab* 2019; 39: 2132–2143.
12. Momjian-Mayor I and Baron JC. The pathophysiology of watershed infarction in internal carotid artery disease: review of cerebral perfusion studies. *Stroke* 2005; 36: 567–577.
13. Yamauchi H, Fukuyama H, Yamaguchi S, et al. High-intensity area in the deep white matter indicating hemodynamic compromise in internal carotid artery occlusive disorders. *Arch Neurol* 1991; 48: 1067–1071.
14. Kaczmarz S, Griese V, Preibisch C, et al. Increased variability of watershed areas in patients with high-grade carotid stenosis. *Neuroradiology* 2018; 60: 311–323.
15. Zarrinkoob L, Wahlin A, Ambarki K, et al. Blood flow lateralization and collateral compensatory mechanisms in patients with carotid artery stenosis. *Stroke* 2019; 50: 1081–1088.
16. Schroeder T. Hemodynamic significance of internal carotid artery disease. *Acta Neurol Scand* 1988; 77: 353–372.
17. Markus HS. Cerebral perfusion and stroke. *J Neurol Neurosurg Psychiatry* 2004; 75: 353–361.

18. Powers WJ, Press GA, Grubb RL Jr, et al. The effect of hemodynamically significant carotid artery disease on the hemodynamic status of the cerebral circulation. *Ann Intern Med* 1987; 106: 27–34.
19. Dirnagl U and Pulsinelli W. Autoregulation of cerebral blood flow in experimental focal brain ischemia. *J Cereb Blood Flow Metab* 1990; 10: 327–336.
20. Hyder F, Shulman RG and Rothman DL. A model for the regulation of cerebral oxygen delivery. *J Appl Physiol* (1985) 1998; 85: 554–564.
21. Hyder F, Kennan RP, Kida I, et al. Dependence of oxygen delivery on blood flow in rat brain: a 7 tesla nuclear magnetic resonance study. *J Cereb Blood Flow Metab* 2000; 20: 485–498.
22. Hyder F, Kida I, Behar KL, et al. Quantitative functional imaging of the brain: towards mapping neuronal activity by BOLD fMRI. *NMR Biomed* 2001; 14: 413–431.
23. Alsop DC, Detre JA, Golay X, et al. Recommended implementation of arterial spin-labeled perfusion MRI for clinical applications: a consensus of the ISMRM perfusion study group and the European consortium for ASL in dementia. *Magn Reson Med* 2015; 73: 102–116.
24. Pillai JJ and Mikulis DJ. Cerebrovascular reactivity mapping: an evolving standard for clinical functional imaging. *AJNR Am J Neuroradiol* 2015; 36: 7–13.
25. Donahue MJ, Dethrage LM, Faraco CC, et al. Routine clinical evaluation of cerebrovascular reserve capacity using carbogen in patients with intracranial stenosis. *Stroke* 2014; 45: 2335–2341.
26. Fisher JA, Venkatraghavan L and Mikulis DJ. Magnetic resonance imaging-based cerebrovascular reactivity and hemodynamic reserve. *Stroke* 2018; 49: 2011–2018.
27. Hirsch NM, Toth V, Forschler A, et al. Technical considerations on the validity of blood oxygenation level-dependent-based MR assessment of vascular deoxygenation. *NMR Biomed* 2014; 27: 853–862.
28. Jespersen SN and Ostergaard L. The roles of cerebral blood flow, capillary transit time heterogeneity, and oxygen tension in brain oxygenation and metabolism. *J Cereb Blood Flow Metab* 2012; 32: 264–277.
29. Ostergaard L, Engedal TS, Moreton F, et al. Cerebral small vessel disease: capillary pathways to stroke and cognitive decline. *J Cereb Blood Flow Metab* 2016; 36: 302–325.
30. Mundiyanapurath S, Ringleb PA, Diatschuk S, et al. Capillary transit time heterogeneity is associated with modified Rankin scale score at discharge in patients with bilateral high grade internal carotid artery stenosis. *PLoS One*. 2016; 11: e0158148.
31. NASCET SC. North American Symptomatic Carotid Endarterectomy Trial. Methods, patient characteristics, and progress. *Stroke* 1991; 22: 711–720.
32. Baudrexel S, Volz S, Preibisch C, et al. Rapid single-scan T2*-mapping using exponential excitation pulses and image-based correction for linear background gradients. *Magn Reson Med* 2009; 62: 263–268.
33. Hirsch NM and Preibisch C. T2* mapping with background gradient correction using different excitation pulse shapes. *AJNR Am J Neuroradiol* 2013; 34: E65–E68.
34. Preibisch C, Castrillon GJ, Buhner M, et al. Evaluation of multiband EPI acquisitions for resting State fMRI. *PLoS One* 2015; 10: e0136961.
35. Kaczmarz S, Gottler J, Kooijman H, et al. Evaluation of pCASL sequences for CBF measures in healthy participants and patients with high-grade internal carotid artery stenosis. In: *ESMRMB 2016, 33rd Annual Scientific Meeting, 29(Suppl 1): S61. Abstract 67*. Vienna, Austria, 29 September–1 October 2016.
36. Fazekas F, Chawluk JB, Alavi A, et al. MR signal abnormalities at 1.5 T in Alzheimer's dementia and normal aging. *AJR Am J Roentgenol* 1987; 149: 351–356.
37. Magerkurth J, Volz S, Wagner M, et al. Quantitative T2*-mapping based on multi-slice multiple gradient echo flash imaging: retrospective correction for subject motion effects. *Magn Reson Med* 2011; 66: 989–997.
38. Welker K, Boxerman J, Kalnin A, et al. ASFNR recommendations for clinical performance of MR dynamic susceptibility contrast perfusion imaging of the brain. *AJNR Am J Neuroradiol* 2015; 36: E41–E51.
39. Kluge A, Lukas M, Toth V, et al. Analysis of three leakage-correction methods for DSC-based measurement of relative cerebral blood volume with respect to heterogeneity in human gliomas. *Magn Reson Imaging* 2016; 34: 410–421.
40. Mutsaerts HJ, Steketee RM, Heijtel DF, et al. Inter-vendor reproducibility of pseudo-continuous arterial spin labeling at 3 Tesla. *PLoS One* 2014; 9: e104108.
41. Garcia DM, Duhamel G and Alsop DC. Efficiency of inversion pulses for background suppressed arterial spin labeling. *Magn Reson Med*. 2005; 54: 366–372.
42. Mutsaerts HJ, Petr J, Vaclavu L, et al. The spatial coefficient of variation in arterial spin labeling cerebral blood flow images. *J Cereb Blood Flow Metab* 2017; 37: 3184–3192.
43. Vondráčková L, Krukowski P and Petr J. Data-driven model for evaluation of cerebrovascular-reserve measurement with hypercapnia BOLD. In: *Proceedings of the 24th annual meeting of ISMRM. Abstract 3801*, Singapore, 7–13 May 2016.
44. Mouridsen K, Hansen MB, Ostergaard L, et al. Reliable estimation of capillary transit time distributions using DSC-MRI. *J Cereb Blood Flow Metab* 2014; 34: 1511–1521.
45. Mouridsen K, Friston K, Hjort N, et al. Bayesian estimation of cerebral perfusion using a physiological model of microvasculature. *Neuroimage* 2006; 33: 570–579.
46. Hayashi T, Watabe H, Kudomi N, et al. A theoretical model of oxygen delivery and metabolism for physiologic interpretation of quantitative cerebral blood flow and metabolic rate of oxygen. *J Cereb Blood Flow Metab* 2003; 23: 1314–1323.
47. Mintun MA, Lundstrom BN, Snyder AZ, et al. Blood flow and oxygen delivery to human brain during functional activity: theoretical modeling and experimental data. *Proc Natl Acad Sci USA* 2001; 98: 6859–6864.
48. Yablonskiy DA and Haacke EM. Theory of NMR signal behavior in magnetically inhomogeneous tissues: the static dephasing regime. *Magn Reson Med* 1994; 32: 749–763.

49. Toth V, Forschler A, Hirsch NM, et al. MR-based hypoxia measures in human glioma. *J Neurooncol* 2013; 115: 197–207.
50. Hedderich D, Kluge A, Pyka T, et al. Consistency of normalized cerebral blood volume values in glioblastoma using different leakage correction algorithms on dynamic susceptibility contrast magnetic resonance imaging data without and with preload. *J Neuroradiol* 2019; 46: 44–51.
51. Leenders KL. PET: blood flow and oxygen consumption in brain tumors. *J Neurooncol* 1994; 22: 269–273.
52. Gibbs JM, Leenders KL, Wise RJS and Jones T. Evaluation of cerebral perfusion reserve in patients with carotid-artery occlusion. *Lancet* 1984; 323: 310–314.
53. Lythgoe DJ, Østergaard L, Williams SCR, et al. Quantitative perfusion imaging in carotid artery stenosis using dynamic susceptibility contrast-enhanced magnetic resonance imaging. *Magn Reson Imaging* 2000; 18: 1–11.
54. Fan AP, Jahanian H, Holdsworth SJ, et al. Comparison of cerebral blood flow measurement with [15O]-water positron emission tomography and arterial spin labeling magnetic resonance imaging: a systematic review. *J Cereb Blood Flow Metab* 2016; 36: 842–861.
55. Fan AP, Guo J, Khalighi MM, et al. Long-delay arterial spin labeling provides more accurate cerebral blood flow measurements in Moyamoya patients: a simultaneous positron emission tomography/MRI study. *Stroke* 2017; 48: 2441–2449.
56. Keil VC, Eichhorn L, Mutsaerts H, et al. Cerebrovascular reactivity during prolonged breath-hold in experienced Freedivers. *AJNR Am J Neuroradiol* 2018; 39: 1839–1847.
57. Waddle SL, Juttukonda MR, Lants SK, et al. Classifying intracranial stenosis disease severity from functional MRI data using machine learning. *J Cereb Blood Flow Metab* 2020; 40: 705–719.
58. Mutsaerts HJ, van Dalen JW, Heijtel DF, et al. Cerebral perfusion measurements in elderly with hypertension using arterial spin labeling. *PLoS One* 2015; 10: e0133717.
59. Sam K, Small E, Poubanc J, et al. Reduced contralateral cerebrovascular reserve in patients with unilateral stenocclusive disease. *Cerebrovasc Dis* 2014; 38: 94–100.
60. Hino A, Tenjin H, Horikawa Y, et al. Hemodynamic and metabolic changes after carotid endarterectomy in patients with high-degree carotid artery stenosis. *J Stroke Cerebrovasc Dis* 2005; 14: 234–238.
61. Kluytmans M, van der Grond J, Folkers PJ, et al. Differentiation of gray matter and white matter perfusion in patients with unilateral internal carotid artery occlusion. *J Magn Reson Imaging* 1998; 8: 767–774.
62. Vagal AS, Leach JL, Fernandez-Ulloa M, et al. The acetazolamide challenge: techniques and applications in the evaluation of chronic cerebral ischemia. *AJNR Am J Neuroradiol* 2009; 30: 876–884.
63. Richter V, Helle M, van Osch MJ, et al. MR imaging of individual perfusion reorganization using superselective pseudocontinuous arterial spin-labeling in patients with complex extracranial steno-occlusive disease. *AJNR Am J Neuroradiol* 2017; 38: 703–711.
64. Juttukonda MR and Donahue MJ. Neuroimaging of vascular reserve in patients with cerebrovascular diseases. *Neuroimage* 2019; 187: 192–208.
65. Mutsaerts HJ, Richard E, Heijtel DF, et al. Gray matter contamination in arterial spin labeling white matter perfusion measurements in patients with dementia. *Neuroimage Clin* 2014; 4: 139–144.
66. van Osch MJ, Teeuwisse WM, van Walderveen MA, et al. Can arterial spin labeling detect white matter perfusion signal? *Magn Reson Med* 2009; 62: 165–173.
67. Baron JC, Bousser MG, Rey A, et al. Reversal of focal “misery-perfusion syndrome” by extra-intracranial arterial bypass in hemodynamic cerebral ischemia. A case study with 15O positron emission tomography. *Stroke* 1981; 12: 454–459.
68. Kety SS and Schmidt CF. The effects of altered arterial tensions of carbon dioxide and oxygen on cerebral blood flow and on cerebral oxygen consumption of normal young men. *J Clin Invest* 1948; 27: 484–492.
69. Vafae MS and Gjedde A. Model of blood–brain transfer of oxygen explains nonlinear flow-metabolism coupling during stimulation of visual cortex. *J Cereb Blood Flow Metab* 2000; 20: 747–754.
70. Germuska M, Chandler HL, Stickland RC, et al. Dual-calibrated fMRI measurement of absolute cerebral metabolic rate of oxygen consumption and effective oxygen diffusivity. *Neuroimage* 2019; 184: 717–728.
71. Buxton RB and Frank LR. A model for the coupling between cerebral blood flow and oxygen metabolism during neural stimulation. *J Cereb Blood Flow Metab* 1997; 17: 64–72.
72. Cirillo M, Capasso G and DeSanto NG. Relationship between hematocrit and blood pressure: implications for primary hypertension. *Nephron* 1993; 65: 505–510.
73. Jae SY, Kurl S, Laukkanen JA, et al. Higher blood hematocrit predicts hypertension in men. *J Hypertens* 2014; 32: 245–250.
74. Calamante F, Christensen S, Desmond PM, et al. The physiological significance of the time-to-maximum (Tmax) parameter in perfusion MRI. *Stroke* 2010; 41: 1169–1174.
75. Marshall RS, Lazar RM, Liebeskind DS, et al. Carotid revascularization and medical management for asymptomatic carotid stenosis – hemodynamics (CREST-H): Study design and rationale. *Int J Stroke* 2018; 13: 985–991.
76. Pittman RN. Oxygen gradients in the microcirculation. *Acta Physiol (Oxf)* 2011; 202: 311–322.
77. Rasmussen PM, Jespersen SN and Østergaard L. The effects of transit time heterogeneity on brain oxygenation during rest and functional activation. *J Cereb Blood Flow Metab* 2015; 35: 432–442.
78. Engedal TS, Hjort N, Hougaard KD, et al. Transit time homogenization in ischemic stroke – a novel biomarker of penumbral microvascular failure? *J Cereb Blood Flow Metab* 2018; 38: 2006–2020.
79. Günther M. Highly efficient accelerated acquisition of perfusion inflow series by cycled arterial spin labeling. In: *Proceedings of the 15th annual meeting of ISMRM*. Berlin, Germany, 19–25 May 2007.

80. van Osch MJ, Teeuwisse WM, Chen Z, et al. Advances in arterial spin labelling MRI methods for measuring perfusion and collateral flow. *J Cereb Blood Flow Metab* 2018; 38: 1461–1480.
81. Magon S, Basso G, Farace P, et al. Reproducibility of BOLD signal change induced by breath holding. *Neuroimage* 2009; 45: 702–712.
82. Watchmaker JM, Frederick BD, Fusco MR, et al. Clinical use of cerebrovascular compliance imaging to evaluate revascularization in patients with Moyamoya. *Neurosurgery* 2019; 84: 261–271.
83. Kanda T, Fukusato T, Matsuda M, et al. Gadolinium-based contrast agent accumulates in the brain even in subjects without severe renal dysfunction: evaluation of autopsy brain specimens with inductively coupled plasma mass spectroscopy. *Radiology* 2015; 276: 228–232.
84. Kaczmarz S, Goettler J, Hock A, et al. Reducing T2-related bias in mq-BOLD derived maps of oxygen extraction fraction by 3D acquisition. In: *Proceedings of the 26th annual meeting of ISMRM. Abstract 5023*, Paris, France, 16–21 June 2018.
85. Gersing AS, Ankenbrank M, Schwaiger BJ, et al. Mapping of cerebral metabolic rate of oxygen using dynamic susceptibility contrast and blood oxygen level dependent MR imaging in acute ischemic stroke. *Neuroradiology* 2015; 57: 1253–1261.
86. Preibisch C, Shi K, Kluge A, et al. Characterizing hypoxia in human glioma: a simultaneous multimodal MRI and PET study. *NMR Biomed* 2017; 30: e3775.
87. Wiestler B, Kluge A, Lukas M, et al. Multiparametric MRI-based differentiation of WHO grade II/III glioma and WHO grade IV glioblastoma. *Sci Rep* 2016; 6: 35142.
88. Nonaka H, Akima M, Hatori T, et al. Microvasculature of the human cerebral white matter: arteries of the deep white matter. *Neuropathology* 2003; 23: 111–118.
89. Kaczmarz S, Gottler J, Zimmer C, et al. Characterizing white matter fiber orientation effects on multi-parametric quantitative BOLD assessment of oxygen extraction fraction. *J Cereb Blood Flow Metab* 2020; 40: 760–774.